Scientific Contributions Oil & Gas, Vol. 49. No. 1, March: 409 - 426

SCIENTIFIC CONTRIBUTIONS OIL AND GAS

Testing Center for Oil and Gas
LEMIGAS

Journal Homepage:http://journal.lemigas.esdm.go.id
ISSN: 2089-3361, e-ISSN: 2541-0520

Multilinear Regression–Based Rock Physics Template Modeling for Sandstone Reservoir Characterization

Muhammad Alif Fahrizi & Sonny Winardhi

Geophysical Engineering, Faculty of Mining and Petroleum Engineering, Institut Teknologi Bandung, Indonesia

Corresponding Author : Muhammad Alif Fahrizi (aliffahrizi@gmail.com)

Manuscript received: January 13th, 2025; Revised: January 26th, 2026
Approved: January 27th, 2026; Available online: March 25th, 2026; Published: March 16th, 2026.

ABSTRACT - Rock Physics Templates (RPT) are widely used to link petrophysical parameters with elastic properties for fluid identification in reservoir characterization. Previous studies have demonstrated the potential of RPT for fluid detection method; however, well-defined procedures for determining rock matrix parameters and P-wave velocity (Vp) as the basis for RPT construction remain limited. This study develops a systematic workflow for RPT construction based on volumetric and rock physics approached, where rock matrix properties are estimated directly from wireline logs when core data is unavailable. The performance of the proposed RPT approach is evaluated through comparing with conventional elastic attribute methods, namely Curved Pseudo Elastic Impedance (CPEI) and Lambda –Rho analysis. The results indicate that the RPT workflow provides improved fluid discrimination than the conventional methods, highlithing its effectiveness as a reliable rock-physics-based tool for fluid identification in sandstone reservoirs.

Keywords: rock physics, acoustic impedance, VpVs Ratio, multi-linear regression.

How to cite this article:

Muhammad Alif Fahrizi and Sonny Winardhi 2026, Multilinear Regression–Based Rock Physics Template Modeling For Sandstone Reservoir Characterization, Scientific Contributions Oil and Gas, 49 (1) pp. 409 - 426. DOI org/10.29017/scog.v49i1.2014

INTRODUCTION

Reservoir characterization aims to qualitatively and quantitatively describe reservoir properties and is commonly conducted through three main stages: geometric delineation, physical property description, and monitoring of property changes during production (Sukmono & Ambarsari, 2019; Hutabarat, et al., 2014; Pangastuti, et al., 2025; Taqiy, et al., 2025). Within this framework, the physical property description stage requires the estimation of petrophysical parameters from wireline log and seismic data (Winardhi et al., 2023). Porosity (Ø) and hydrocarbon fluid saturation (SFL) are the primary target properties, where porosity represents the pore volume within the rock, and fluid saturation reflects the proportion of hydrocarbon and non-hydrocarbon fluids occupying the pore space.

With advances in seismic data quality, quantitative approaches have increasingly been adopted to estimate reservoir properties, one of which is the Rock Physics Template (RPT) (Ryannugroho, et al., 2025; Hutami, et al., 2019). First introduced by Odegaard and Avseth (2004), RPT is an interpretation tool that integrates elastic parameters, commonly acoustic impedance (AI) and the Vp/Vs ratio, to infer lithology and pore-fluid variations by incorporating geological controls such as depositional environment, diagenesis, and fluid saturation effects. RPTs are theoretically formulated through rock physics modeling while integrating local geological constraints. Their construction involves the integration of several rock physics concepts, including rock physics models (e.g., friable-sand, contact cement, and constant cement models), elastic bounding methods (Voigt–Reuss–Hill and Hashin–Shtrikman), Gassmann's fluid substitution, and Backus averaging (Avseth et al., 2010; Boruah, 2010). Through these relationships, RPT provides a framework for linking elastic attributes to petrophysical properties, thereby facilitating lithology and fluid interpretation.

Despite its utility, conventional RPT construction is often constrained by the requirement for extensive datasets, which may not always be available in practice, the reby limiting its applicability in many field cases. To address this limitation, Fawad and Mondol (2022) proposed a simplified RPT approach with reduced data requirements. However, their interpretation framework does not fully adhere to Gassmann's theory, particularly regarding the influence of hydrocarbon fluid saturation on the Vp/Vs ratio. This limitation motivates further development of quantitative RPT-based approaches that remain physically consistent while reducing data dependency.

Pranatikta and Winardhi (2025) addressed the limitation of the RPT proposed by Fawad and Mondol (2022) by incorporating Gassmann's fluid substitution effects (Gassmann, 1951), thereby restoring the physical consistency between fluid saturation and the Vp/Vs ratio. However, their proposed RPT framework does not provide a clear procedural workflow for deriving matrix elastic parameters, particularly matrix density and P-wave velocity. Consequently, the practical application of the Pranatikta and Winardhi (2025) RPT remains limited. This study aims to bridge these gaps by establishing a systematic, log-based procedure for matrix parameter estimation.

METHODOLOGY

Data Availability

The data used in this study consist of two wells, SL-1 and SL-2, which contain limited volumetric logs. An additional well, LSE-1120, is included as a reference of a well with a complete volumetric log dataset. An overview of the available data is presented in Figure 1.

Matrix Parameter

The application of the Rock Physics Template (RPT) proposed by Pranatikta and Winardhi requires matrix elastic parameters, particularly matrix density and P-wave velocity. Conventionally, these parameters are obtained from laboratory measurements on core samples. However, core data are not always available, as not all wells provide samples suitable for laboratory testing. To overcome this limitation, this study utilizes a multilinear regression (MLR)

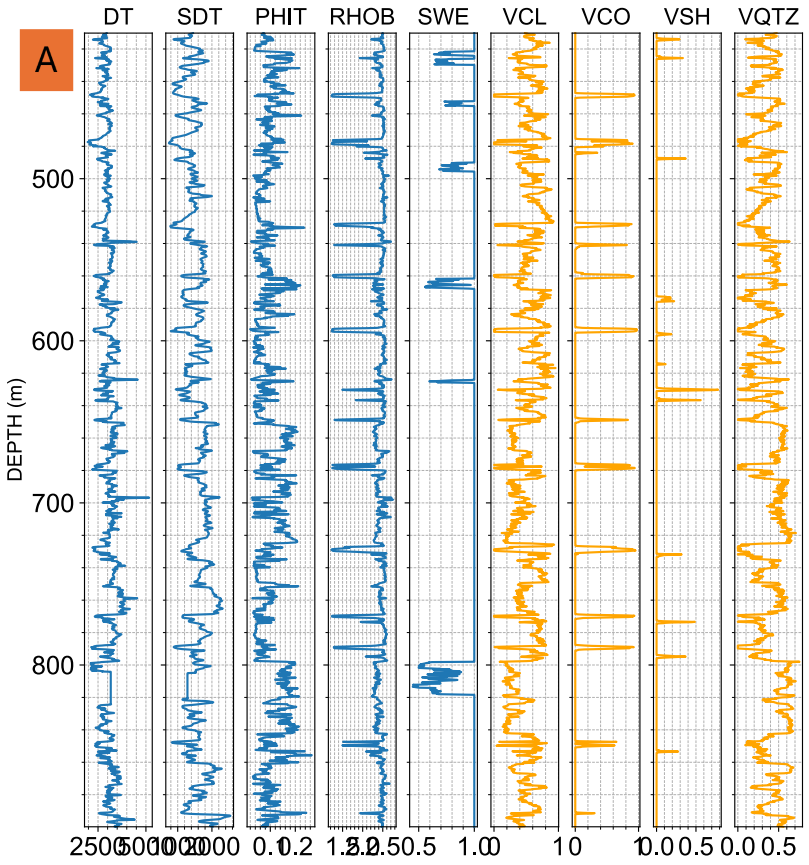
A
DT
SDT
PHIT
RHOB
SWE
VCL
VCO
VSH
VQTZ
DEPTH (m)
500
600
700
800

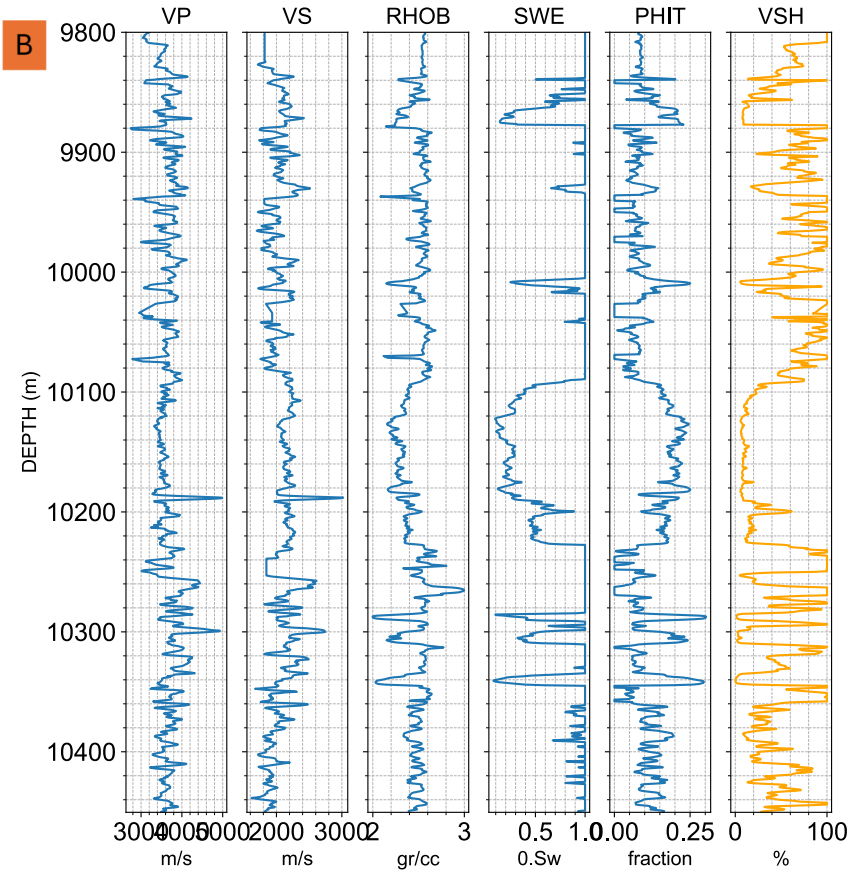
B
VP
VS
RHOB
SWE
PHIT
VSH
DEPTH (m)
9800
9900
10000
10100
10200
10300
10400
m/s
m/s
gr/cc
0.Sw
fraction
%

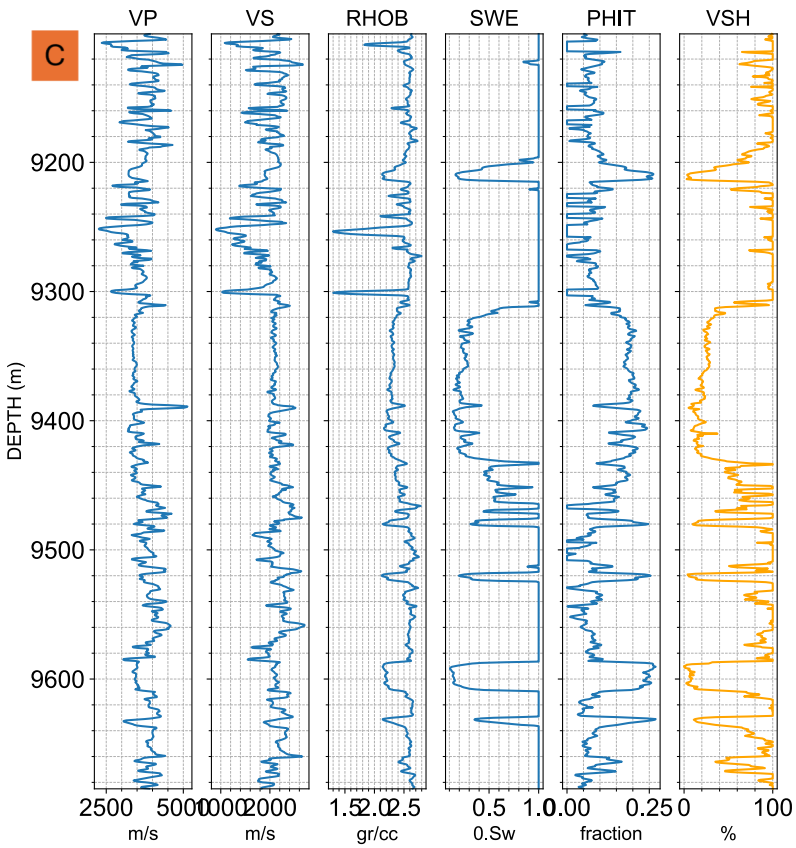

Figure 1. Well log data from (A) LSE-1120, (B) SL-1, and (C) SL-2. The orange color represents volumetric logs.

framework to derive intrinsic matrix elastic parameters directly from wireline log data, thereby eliminating the dependency on laboratory measurements and enabling broader applicability of the proposed RPT framework.

To estimate matrix density using the multilinear regression (MLR) approach, Equation (1) is applied. This equation is derived from the bulk density formulation and expresses matrix density as a volumetric-weighted combination of individual rock constituents. Through this formulation, matrix density is estimated for each rock type based on its volumetric contribution, enabling the regression framework to determine the optimal matrix density values that best fit the observed log data.

$$\frac{\rho_b - \phi SW\rho_w - \phi(1-SW)\rho_{hc}}{(1-\phi)} = \rho_{ma} = \sum_i \rho_i V_i \quad (1)$$

Where ρb denotes the bulk density obtained from density logs, ϕ represents porosity, SW is water saturation, ρw is the density of formation water, and $\rho_h c$ is the density of hydrocarbon fluids. The term $\rho_m a$ corresponds to the matrix density, which represents the density of the solid rock framework excluding pore fluids. The right-hand side of the equation expresses the matrix density as a volumetric-weighted sum of the densities of individual mineral constituents (ρ_i), where V_i denotes the volumetric fraction of each constituent mineral.

The remaining parameter required under matrix conditions is the P-wave velocity (V_p). To estimate the matrix P-wave velocity for each rock type, Wyllie's time-average equation is employed. Equation (2) is used to derive the matrix Vp of each rock by removing the fluid contribution from the measured P-wave velocity, thereby providing an estimate of the intrinsic elastic velocity of the solid rock matrix.

$$\frac{\frac{1}{V_P} - \frac{\phi}{V_{P_{fl}}}}{(1-\phi)} = \frac{1}{V_{P_{ma}}} = \sum_i \frac{V_i}{V_{P_i}} \quad (2)$$

Where V_p denotes the measured P-wave velocity obtained from sonic or seismic data. The term $V_p fl$ represents the effective P-wave velocity of the pore fluid. The parameter $V_p ma$ corresponds to the matrix

P-wave velocity, representing the intrinsic P-wave velocity of the solid rock framework under matrix conditions. On the right-hand side of the equation, V_i denotes the volumetric fraction of each mineral constituent, and V_{Pi} represents the P-wave velocity of the corresponding mineral. This formulation follows Wyllie's time-average concept, in which the reciprocal of P-wave velocity is assumed to vary linearly with the volumetric fractions of the rock constituents.

Equations 1 and 2 are used to estimate the matrix conditions of each rock type within the multilinear regression (MLR) framework. In this study, MLR is specifically applied as a decoupling operator to isolate matrix-controlled elastic responses from volumetric effects. Mathematically, the MLR formulation is expressed in Equation 3.

$$y = \sum_i W_i X_i \tag{3}$$

Where y represents the dependent variable to be estimated, X_i denotes the i-th independent input variable, and W_i is the corresponding regression coefficient. The summation indicates that the predicted output is expressed as a linear combination of all input variables. Within the multilinear regression framework, the coefficients W_i are determined by minimizing the misfit between predicted and observed values, allowing the model to quantify the relative contribution of each input parameter to the estimated matrix property.

Rock physics template pranatikta and winardhi (2025)

The RPT proposed by Pranatikta and Winardhi (2025) is a modified version of the RPT developed by Fawad and Mondol (2022). Both RPT approaches are based on Wyllie's time average equation and bulk density equation. To estimate hydrocarbon fluid saturation using both RPT models, Equation (4) is applied.

Pranatikta & Winardhi (2025) incorporated the Gassmann fluid substitution effect into the RPT framework of Fawad and Mondol (2022), resulting a modified porosity formulation presented Equation (5) (Lee, 2003; Wyllie et al. 1951).

$$S_{FL} = \frac{\left\{\begin{matrix}\rho_{ma} + \phi(\rho_w - \rho_{ma}) \\ -AI\left[\frac{1}{V_{p_{ma}}} + \phi\left(\frac{1}{V_{p_w}} - \frac{1}{V_{p_{ma}}}\right)\right]\end{matrix}\right\}}{\left\{\phi\left[AI\left(\frac{1}{V_{p_{hc}}} - \frac{1}{V_{p_w}}\right) - (\rho_{fl} - \rho_w)\right]\right\}} \tag{4}$$

Where S_{FL} represents hydrocarbon fluid saturation and AI denotes acoustic impedance.

$$\phi = 1 - \left\{\frac{V_{s_{sat}}^2 \rho_{sat}}{\left[G^2 \alpha^2 V_{p_{ma}}^2 \rho_{ma}\right]}\right\}^{\frac{1}{2n+1}} \tag{5}$$

Where $V_s sat$ is S-wave velocity in saturated condition, and ρsat represents density under saturated conditions (i.e., bulk density). The parameter α denotes the ratio between S-wave matrix velocity and P-wave matrix velocity ($V_s ma$ / $V_p ma$). The parameters G and n are fitting constants derived from the RPT model. Equation (5) can be arranged into a formulation expressed in terms of, V_s as shows in Equation (6). The V_s model can then be used to determine the optimal fitting parameters that best describe the relationship between fluid saturation and S-wave velocity.

$$V_{S_{sat}} = \sqrt{\frac{\rho_{ma}(1-\phi)}{\rho_{bulk}}} V_{P_{ma}} [G\alpha(1-\phi)^n] \tag{6}$$

RESULT AND DISCUSSION

Results from LSE-1120 (complete volumetric case)

Well LSE-1120 is used as a reference example for the application of the Pranatikta and Winardhi (2025) RPT. This well contains complete volumetric data, allowing the Pranatikta and Winardhi (2025) RPT to be constructed under ideal conditions. The volumetric data available in well LSE-1120 include shale, organic shale, quartz, and coal.

Equation (1) is modeled using the multilinear regression formulation described in Equation (3), resulting in estimated matrix densities for quartz, shale, coal, and organic shale of 2.6202 g/cc, 2.5066 g/cc, 1.1824 g/cc, and 1.3392 g/cc, respectively. Bulk density (ρ_b) is then modeled,

assuming a gas density of 0.2 g/cc and a water density of 1.0 g/cc. The resulting bulk density model achieves a mean absolute error (MAE) of 0.0335, as shown in Figure 2 (C).

Using Equation (2) in conjunction with the multilinear regression (MLR) formulation in Equation (3), the estimated matrix P-wave velocities for quartz, shale, coal, and organic shale are 6042.68 m/s, 3405.88 m/s, 2189.18 m/s, and 2057.03 m/s, respectively. These estimated matrix P-wave velocities produce a MAE of 347.6096, as shown in Figure 2 (D).

The final parameter to be modeled is the S-wave velocity (Vs). Vs is estimated using Equation (6), with the fitting parameters G and n determined through a grid-search procedure. The optimal values obtained are $G = 1.15$ and $n = 2.70$. This model yields a MAE of 206.67, as shown in Figure 2 (E).

Based on the estimated V_p, V_s, and density models, acoustic impedance (AI) and the V_p/V_s ratio are subsequently derived, enabling analysis within the AI–Vp/Vs domain. The complete modeling results for well LSE-1120 are presented in Figure 2.

Based on the results from well LSE-1120, it can be concluded that the Pranatikta & Winardhi (2025) RPT, when combined with matrix parameters estimated using the MLR approach, shows good agreement with the observed data. Given these encouraging results, further analysis is subsequently conducted on well SL-1.

Results from SL-1 (limited volumetric case)

Well SL-1 contains incomplete volumetric log data. In particular, the coal interval in SL-1 does not have volumetric logs, which poses a challenge for both MLR modelling and the Pranatikta and

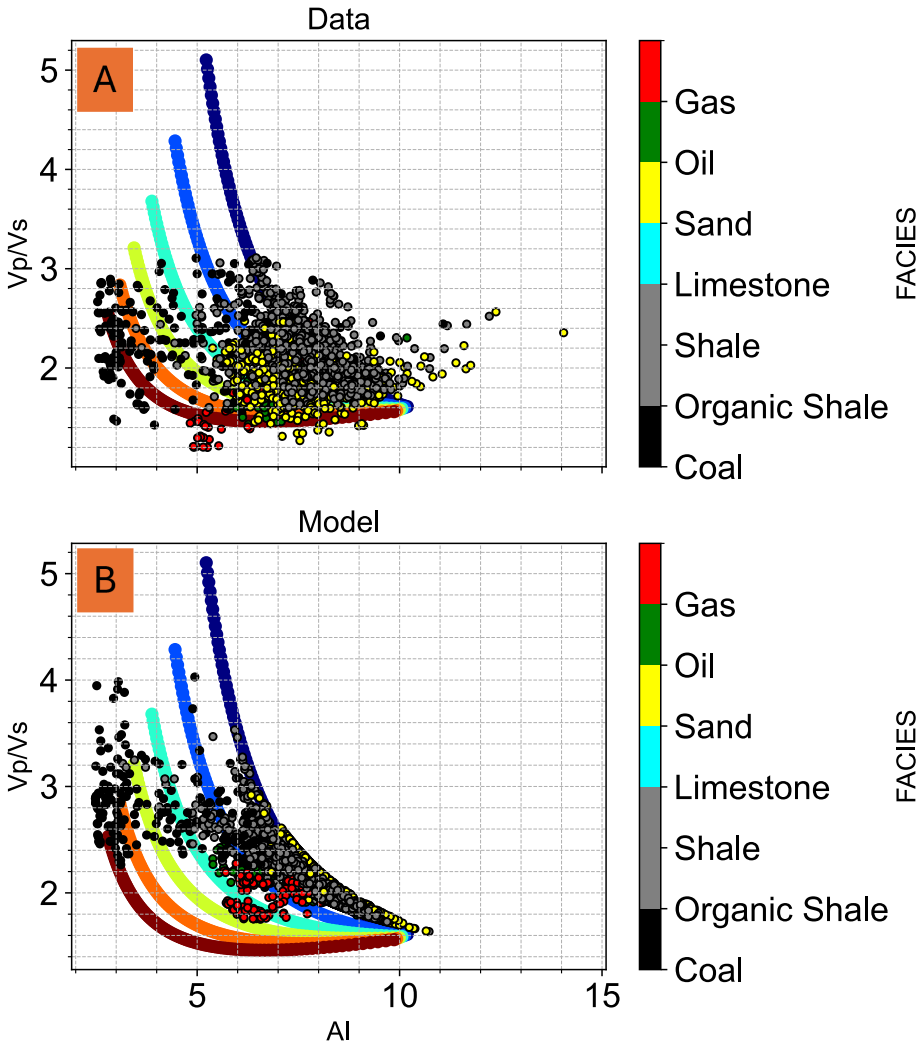

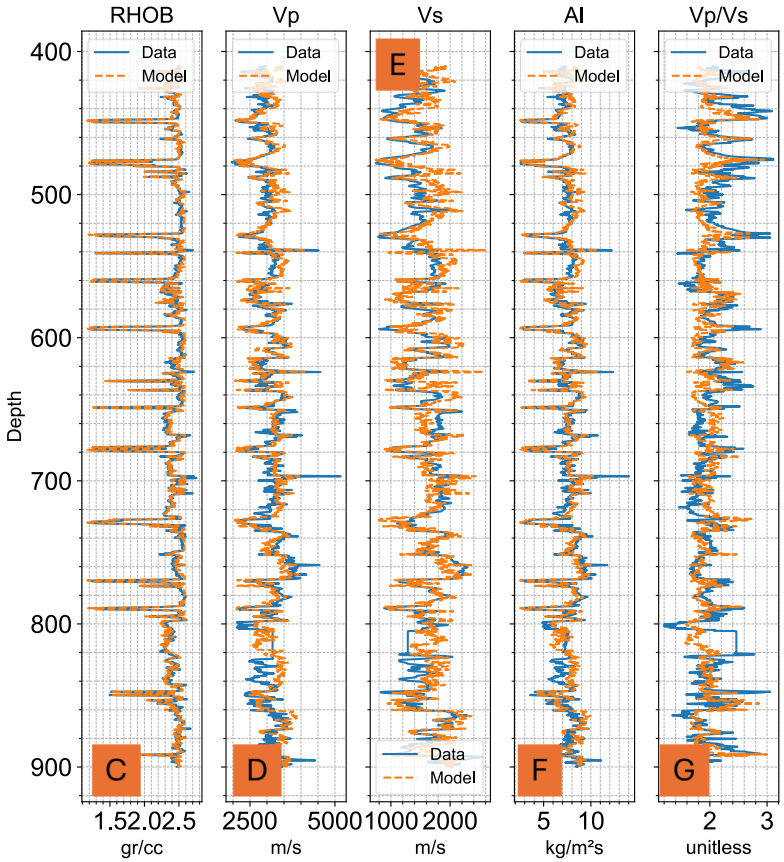

Figure 2. (A) Crossplot of acoustic impedance (AI) versus Vp/Vs ratio from the observed data, overlaid with the constructed Rock Physics Template (RPT). (B) AI–Vp/Vs ratio crossplot from the modeled data, overlaid with the same RPT. (C) Density (RHOB), (D) P-wave velocity (Vp), (E) S-wave velocity (Vs), (F) acoustic impedance (AI), and (G) Vp/Vs ratio logs comparing the model results and observed data at LSE-1120. In panels (C)–(G), the observed data are shown as solid blue lines, while the model results are shown as dashed orange lines.

Winardhi (2025) RPT framework that rely on volumetric information. The only available volumetric data in SL-1 correspond to shale. By applying MLR to model bulk density (ρ_b) without coal volumetrics, the results shown in Figure 3 are obtained using a water density of 1 g/cc and a fluid (oil) density of 0.73 g/cc.

Under the assumption that the rock matrix is primarily composed of quartz and shale, the estimated densities for quartz and shale are 2.6590 g/cc and 2.7025 g/cc, respectively. The estimated shale density is higher than typical shale density values, which are generally around 2.5 g/cc. Therefore, in this study, the term “shale” is treated as a non-reservoir lithology to prevent potential misinterpretation of reservoir quality.

Considering the low coal density observed in well LSE-1120, model errors in ρ_b characterized by non-reservoir densities but exhibiting low density values in the data can be identified and interpreted as coal. This indicates that the shale volumetric log in SL-1 implicitly includes the volumetric contribution of coal.

To estimate the coal volumetric fraction, a modified form of bulk density equation is applied, as presented in Equation (7).

$$V_{coal} = \frac{\rho_b - \phi(SW\rho_w + (1-SW)\rho_{hc}) - (1-\phi)[V_{qtz}\rho_{qtz} + V_{nr}\rho_{nr}]}{(1-\phi)V_{nr}(\rho_{coal} - \rho_{nr})} \quad (7)$$

In this formulation, the solid matrix term is composed of quartz and non-reservoir lithologies, represented by volumetric fractions $Vqtz$ and Vnr, with corresponding densities ρqtz and ρnr. The denominator accounts for the density contrast between coal ($\rho coal$) and non-reservoir lithology,

scaled by the non-reservoir volumetric fraction. The estimated coal volumetric fraction, using coal density obtained from LSE-1120, is shown in Figure 4 (A).

The model successfully accounts for intervals containing coal. However, several depth intervals exhibit higher density values than those predicted by the model. Due to these elevated density values, limestone was initially suspected as the cause. Nevertheless, the gamma-ray response in these intervals is relatively high, suggesting that the lithology is unlikely to be limestone, as shown in Figure 5 (B). Consequently, this lithology cannot be explicitly defined and is hereafter referred to as "x".

The density value used to calculate the volumetric fraction of component "x" is pragmatically defined as the maximum observed bulk density (2.9975 g/cm³). This value is not assigned based on a definitive lithological interpretation, but rather imposed as a statistical upper-bound constraint, analogous to the coal volumetric formulation. The selection of the maximum bulk density reflects the absence of conclusive information regarding the lithological identity of component "x" and serves to ensure volumetric closure, such that the total volumetric fractions of all rock constituents sum to unity.

The resulting "x" volumetric distribution is presented in Figure 5. Bulk density modeling for well SL-1 shows satisfactory agreement with the measured data. By integrating the volumetric constraints derived from the density modeling, the corresponding volumetric logs are generated and shown in Figure 6 C.

With the complete volumetric information obtained, the modeling procedure is continued to the estimation of V_p. V_p The modeling is performed using Equation 2 through the MLR approach. The estimated matrix parameters obtained from the regression are: $\rho qtz = 2.6590$ gr/cc, $\rho sh = 2.7025$ gr/cc, $\rho coal = 1.1824$ gr/cc, and $\rho x = 2.9975$ gr/cc. The resulting modeling is shown in Figure 6 (D).

S-wave velocity (V_s) modeling is performed using Equations (6), employing parameters G and n that are capable of representing both V_s and SW within the AI and V_p/V_s ratio domains. The optimal values of G and n that best represent SW are 1.02 and 3.03, respectively. The resulting V_s model is presented in Figure 6 (E), with a MAE of 200.4285.

Figure . (A) Crossplot of acoustic impedance (AI) versus Vp/Vs ratio from the observed data overlaid with the constructed Rock Physics Template (RPT). (B) AI–Vp/Vs ratio crossplot from the modeled data overlaid with the same RPT. (C) Density (RHOB), (D) P-wave velocity (Vp), (E) S-wave velocity (Vs), (F) acoustic impedance (AI), and (G) Vp/Vs ratio logs comparing model results and observed data for well SL-1. In panels (C)–(G), the observed data are shown as solid blue lines, while the model results are shown as dashed orange lines.

The Xu and Payne model utilizes porosity-ratio aspects to achieve a better fit with observed data (Li et al., 2020; Xu & Payne, 2009). Inspired by the Xu–Payne formulation, this study proposes an approach to further align the model with the observed data. To accomplish this, the model is scaled by a porosity-related term to improve its agreement with observations. Accordingly, a scaling parameter is introduced, which is mathematically expressed in Equation (8). Equation (8) defines a scaling factor used to integrate empirical observations with the theoretical $V_p$model thereby producing a closer to the measured $V_p$data.

$$V_{P_{scaler}} = \frac{V_{P_{data}}}{V_{P_{model}}} \quad (8)$$

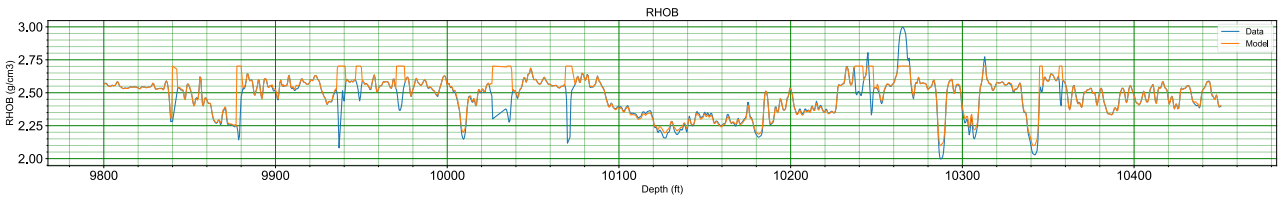

Figure 3. Density model (orange line) compared with the observed density log (blue line) before volumetric adjustment.

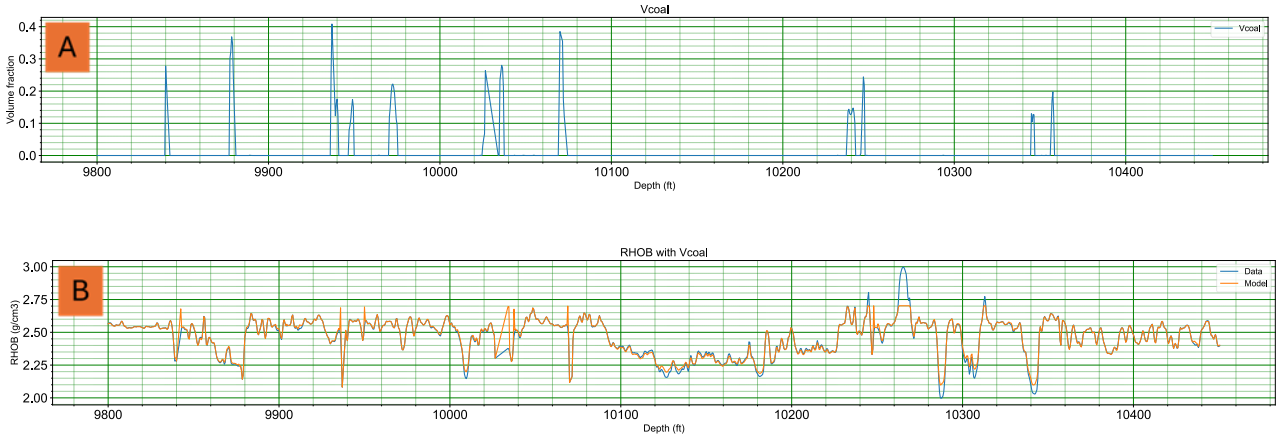

Figure 4. (A) Estimated V_{coal} from Equation (7) and (B) modeled density after V_{coal} available in SL-1.

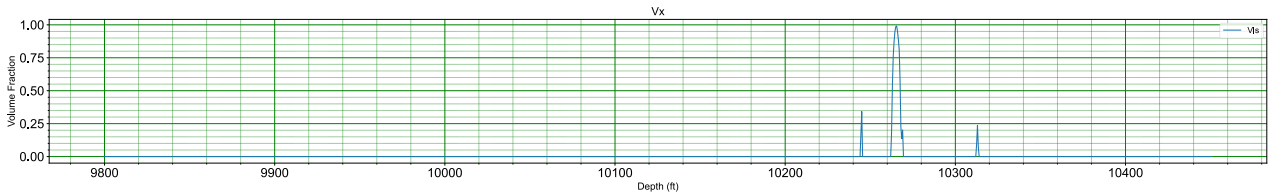

Figure 5. Volumetric distribution of component “x”.

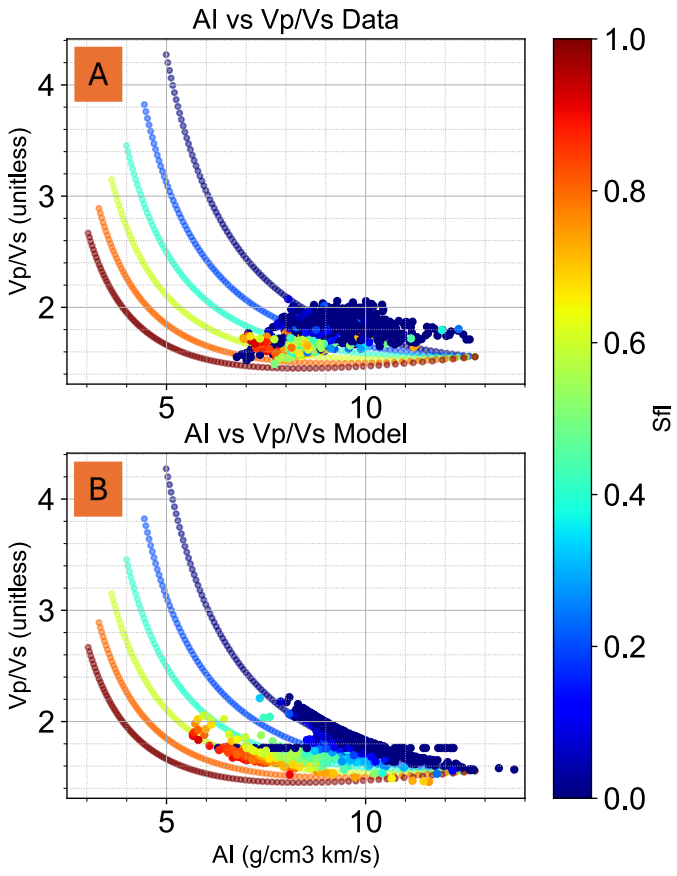

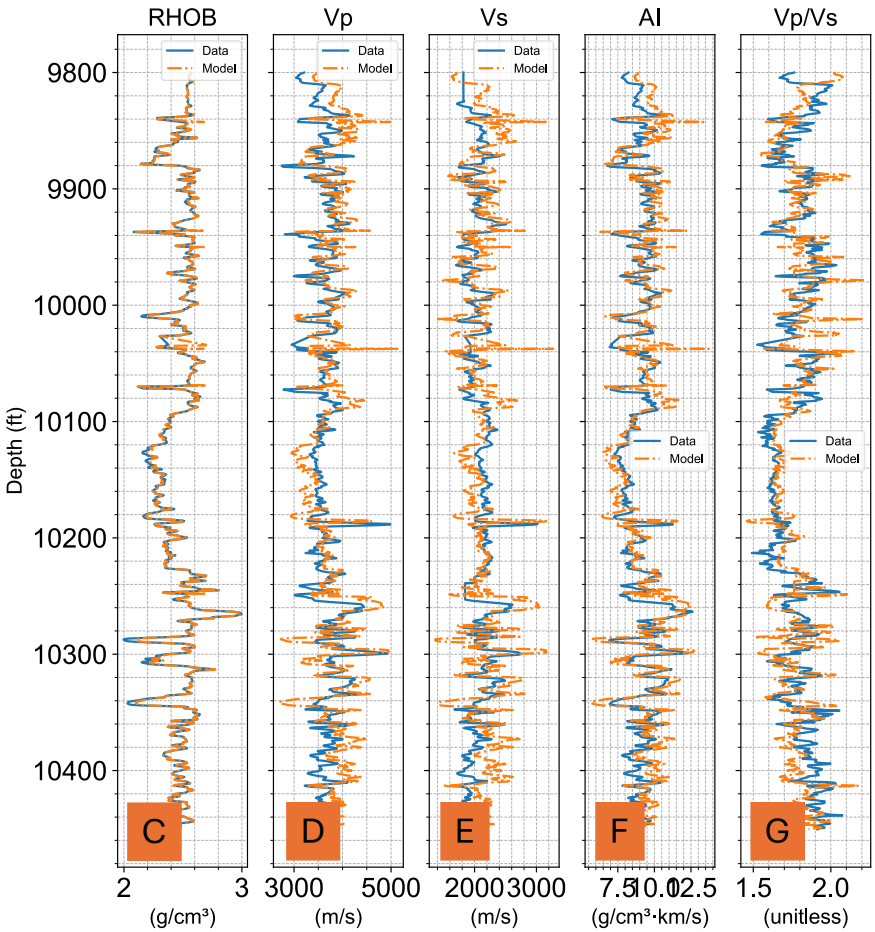

Figure 6. (A) Crossplot of acoustic impedance (AI) versus Vp/Vs ratio from the observed data overlaid with the constructed Rock Physics Template (RPT). (B) AI–Vp/Vs ratio crossplot from the modeled data overlaid with the same RPT. (C) Density (RHOB), (D) P-wave velocity (Vp), (E) S-wave velocity (Vs), (F) acoustic impedance (AI), and (G) Vp/Vs ratio logs comparing model results and observed data for well SL-1. In panels (C)–(G), the observed data are shown as solid blue lines, while the model results are shown as dashed orange lines.

A $V_p scaler$ value close to 1 indicates that the modeled P-wave velocity closely matches the observed data. Increasing $V_{P\ \text{scaler}}$ imply that the modeled P-wave velocity ($V_{P\ \text{model}}$) is lower than the measured P-wave velocity ($V_{P\ \text{data}}$), and vice versa. Figure 7 (A) demonstrates a positive correlation between $V_{P\ \text{scaler}}$ and porosity. By incorporating volumetric color keys, $V_{P\ \text{scaler}}$ exhibits a strong relationship when modeled using porosity in combination with volumetric information. This result indicates that MLR can be effectively utilized to derive a more accurate porosity and volumetric based $V_{P\ \text{scaler}}$ model.

The MLR modeling is performed using porosity and volumetric fractions as independent variables. The resulting $V_{P\ \text{scaler}}$ model, obtained using Equation (9), is presented in Figure 7 (B).

$$V_{P_{scaler}} = 1.0000 + 1.0035\phi - 0.1799V_{qtz} - 0.0836V_{sh} + 0.1094V_{co} - 0.0045V_x \quad (9)$$

The MLR used to derive Equation (9) constrains the intercept to a value of 1 to ensure that the V_{Pma} modeling is already appropriately represented. The application of the resulting $V_{P\ \text{scaler}}$ model is shown in Figure 7 (C), yielding a MAE of 196.3101.

A scaling process is applied to the V_S model to ensure consistency with the observed V_p/V_s ratio. The scaling formulation is kept identical to that used for the V_p model in order to maintain the stability of the V_p/V_s ratio. The scaled V_s model is presented in Figure 8 (E), yielding a MAE of 162.4098. The scaling process demonstrates an improved level of agreement between the modeled and observed data. These results support the

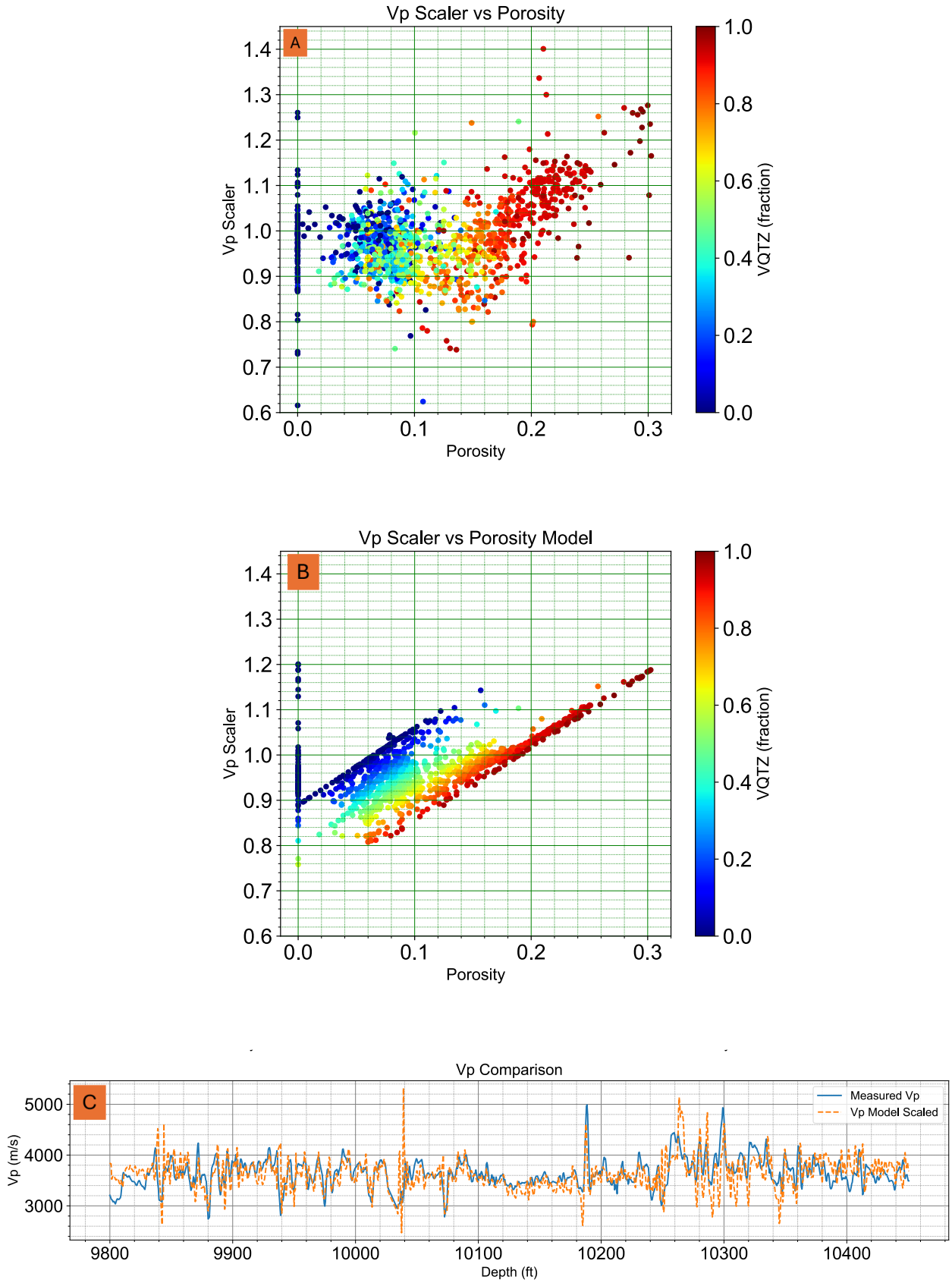

Figure 7. (A) $V_{P\ scaler}$ derived from the observed data, (B) $V_{P\ scaler}$ modeled using porosity and volumetric fractions of each rock, and (C) $V_{P\ model}$ scaled using Equation (9) for well SL-1.

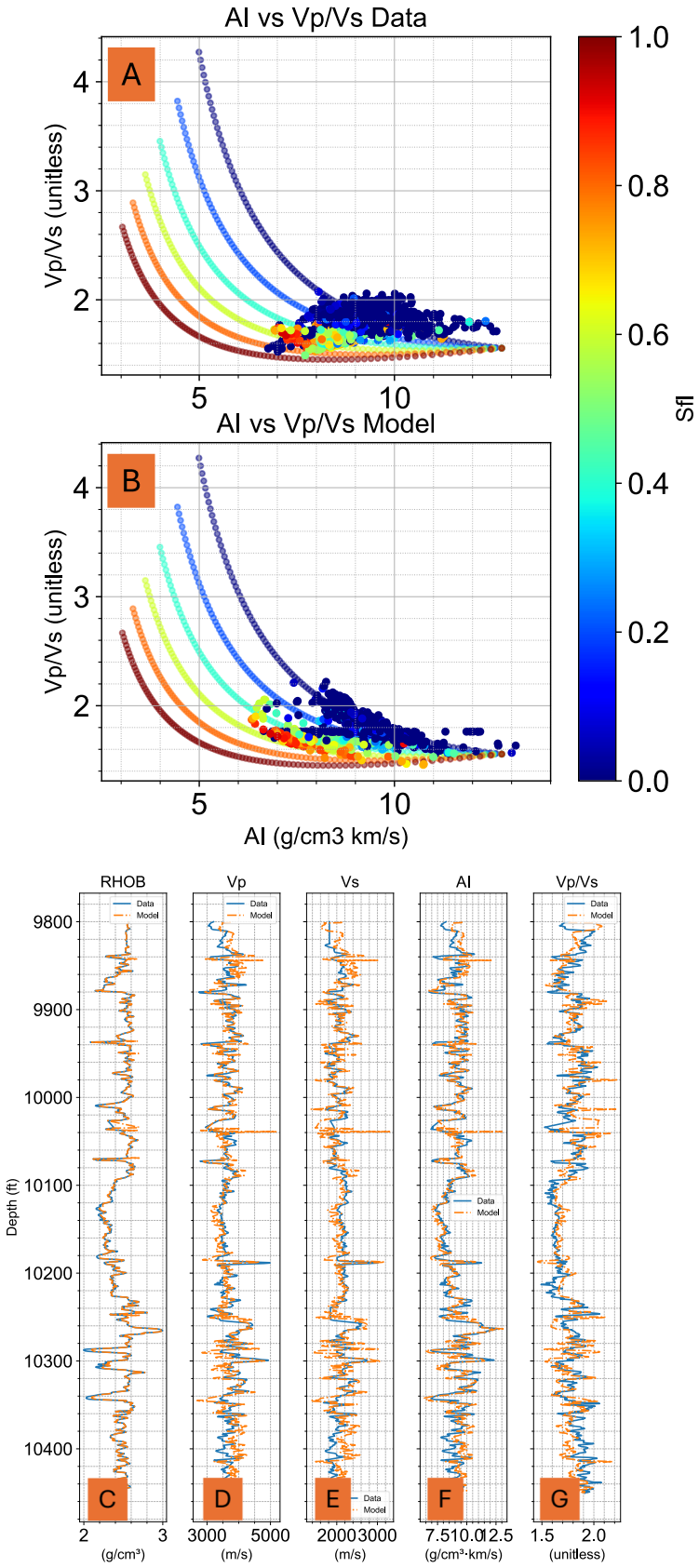

Figure 8. (A) Crossplot of acoustic impedance (AI) versus Vp/Vs ratio from the data overlaid with the constructed rock physics template (RPT). (B) AI–Vp/Vs ratio crossplot from the scaled model overlaid with the same RPT. (C) Density (RHOB), (D) P-wave velocity (Vp), (E) S-wave velocity (Vs), (F) acoustic impedance (AI), and (G) Vp/Vs ratio logs comparing scaled model results and observed data for well SL-1. In panels (C)–(G), the observed data are shown as solid blue lines, while the scaled model results are shown as dashed orange lines.

inclusion of a scaling step in the Pranatikta and Winardhi (2025) RPT modeling workflow.

At this stage, the modeling workflow has produced bulk density (ρ_b), P-wave velocity (V_p), and S-wave velocity (V_s). Consequently, analysis within the acoustic impedance (AI) and V_p/V_s ratio domains can be performed. The Pranatikta and Winardhi (2025) RPT is applied to the data, and the results for the scaled models are presented in Figure 8.

Results from SL-2 (model validation case)

Well SL-2 is used as a case study for V_s modeling in the absence of measured V_s data, as well as a validation well for the SL-1. The modeling is performed using parameters previously obtained from the SL-1 analysis. This approach is considered valid due to the similar geological setting and close spatial proximity between wells SL-1 and SL-2.

The volumetric adjustment for well SL-2 is conducted following the same rationale applied to SL-1, namely the limitation of available volumetric data. By using the same matrix densities (ρ_i) values derived from SL-1, the volumetric fractions of coal and the unidentified rock component "x" are estimated, as shown in Figure 9.

Through the applied volumetric adjustment, a bulk density model is obtained, as shown in Figure 10 (A). The model yields a MAE of 0.0142. This result indicates that the matrix densities (ρ_i) model developed from SL-1 is capable of representing the matrix properties and can be effectively applied to SL-2.

The V_p modeling for SL-2 is performed using the V_{Pi} parameters obtained from SL-1, combined with the volumetric parameters of SL-2. The resulting V_P model shows a MAE of 273.5438. The V_s modeling is conducted using volumetric inputs and the parameters G and n, which were calibrated from the SL-1 well.

The scaling process is applied to the model using Equation (9). The scaled results for V_p are shown in Figure 10 (B), yielding a MAE of 226.0826. For, V_s the MSE values are 228.9122 for the initial V_s model and 189.9537 for the scaled V_s model. In both cases, the scaling procedures demonstrates improved agreement compared to the initial model.

The V_s modeling is subsequently followed by SW modeling. The SW modeling is conducted within the AI and V_p/V_s ratio domains. This modeling is evaluated under several scenarios: 1). using complete elastic data (ρb, V_s, and V_p); 2). using partial data (ρb and V_p) combined with scaled V_s; and 3). using fully modeled elastic parameters. The distributions of AI and Vp/Vs ratio for each scenario are shown in Figures 11.

The complete elastic-data scenario is used to validate the modeling results derived from SL-1. The partial-data scenario with scaled V_s is employed to evaluate the ability of the scaled V_s to represent the actual V_s data. Meanwhile, the scenario using fully modeled parameters is applied to assess the consistency of the resulting model with the Pranatikta and Winardhi (2025) RPT.

The application of the SL-1 model to SL-2, as shown in Figure 11 (A), reproduces the results reasonably well. The fluid distribution in the AI and Vp/Vs ratio domains also occupies the expected locations.

The direct application of the scaled V_s in the partial-data scenario, as shown in Figure 11 (B), exhibits limitations in accurately representing actual data points. Compared with the elastic-data scenario, data points with S_{FL} values close to zero

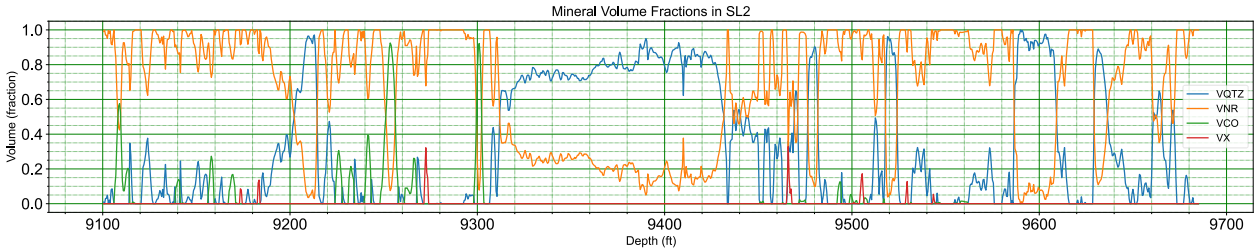

Figure 9. Mineral volumetric fraction of each rock in well SL-2.

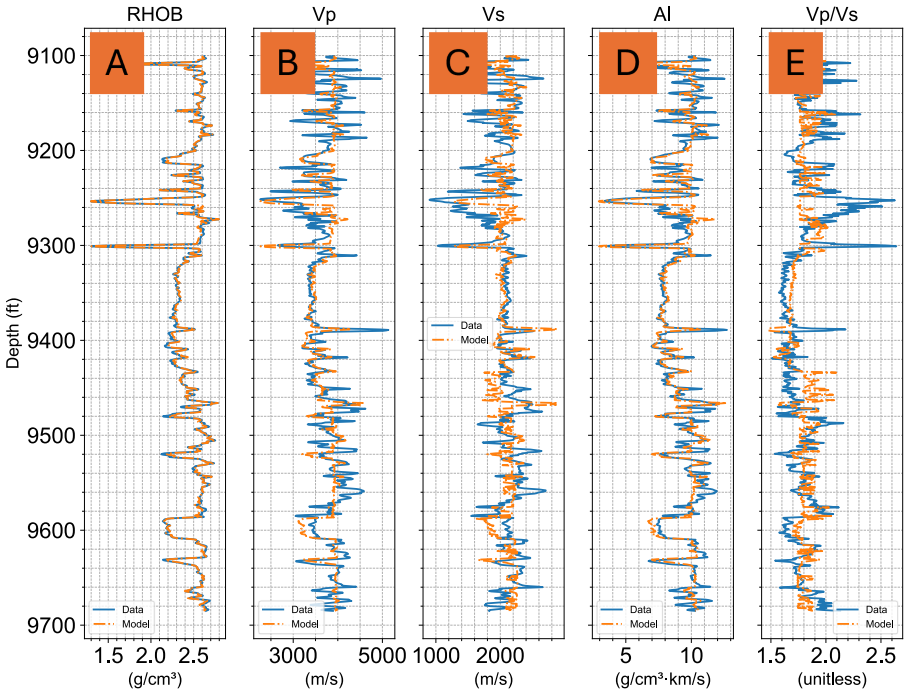

Figure 10. (A) Density (RHOB), (B) P-wave velocity (Vp), (C) S-wave velocity (Vs), (D) acoustic impedance (AI), and (E) Vp/Vs ratio logs, comparing scaled model results and observed data for well SL-2. Observed data are shown as solid blue lines, while the scaled model results are shown as dashed orange lines.

tend to shift toward lower Vp/Vs ratios. This shift leads the Pranatikta and Winardhi (2025) RPT to interpret zones with low Vp/Vs ratios as potential hydrocarbon-bearing intervals. Therefore, the use of scaled V_s cannot be considered a direct substitute for the availability of measured V_s data.

The application of fully modeled elastic parameters, as shown in Figure 11 (C), yields satisfactory results. The fluid distribution is consistent with the Pranatikta and Winardhi (2025) RPT framework. Nevertheless, several spikes similar to those observed in the elastic-data scenario are still present. These spikes are attributed to coal intervals that intersect the fluid saturation lines of the Pranatikta and Winardhi (2025) RPT. This linear pattern arises because the porosity data used characterize coal as zones with zero porosity.

The results from well LSE-1120 demonstrate the critical role of volumetric logs in constructing the Pranatikta and Winardhi (2025) RPT. The analysis of SL-1 further indicates that the incorporation of porosity- and volumetric-based scaling significantly improves model performance compared to the unscaled approach. The validation conducted using SL-2 confirms the robustness of the model derived from SL-1 and and supports the effectiveness of the proposed scaling strategy. Collectively, these results demonstrate that the MLR-based workflow not only enables the estimation of matrix parameters under limited data conditions but also introduces additional modeling steps that enhance the applicability and reliability of the Pranatikta and Winardhi (2025) RPT.

Comparison with another fluid detection method

A comparison is conducted between the Pranatikta and Winardhi (2025) RPT and other fluid-detection methods, namely CPEI (Palgunadi et al., 2016; Pranatikta, et al., 2024; Winardhi et al., 2023) and Lambda–Rho (Goodway, et al., 1997), using well SL-1 as the case study. As the value ranges of CPEI and Lambda–Rho differ from those of fluid saturation, min–max scaling is applied.

To further improve the MAE of both methods, cutoff values are additionally introduced to better replicate the fluid saturation distribution. The resulting MAE values, from lowest to highest, are obtained for the Pranatikta and Winardhi (2025) RPT,

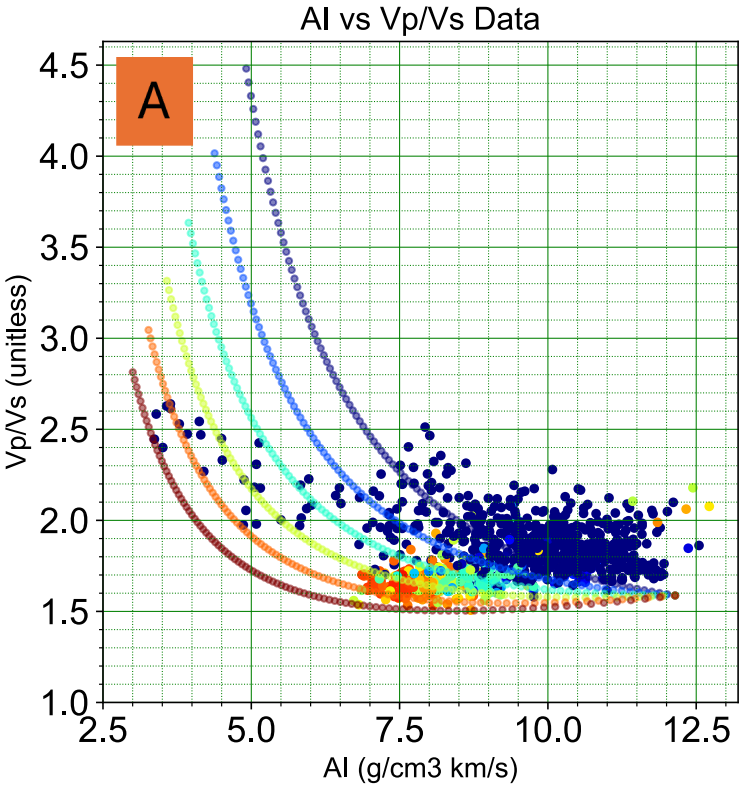
AI vs Vp/Vs Data
A
Vp/Vs (unitless)
4.5
4.0
3.5
3.0
2.5
2.0
1.5
1.0
2.5
5.0
7.5
10.0
12.5
AI (g/cm3 km/s)

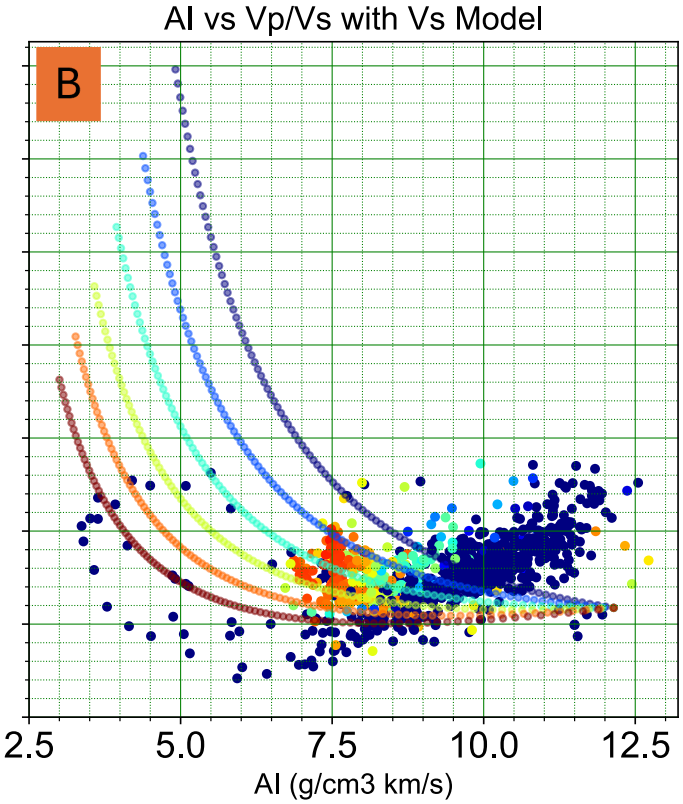
AI vs Vp/Vs with Vs Model
B
2.5
5.0
7.5
10.0
12.5
AI (g/cm3 km/s)

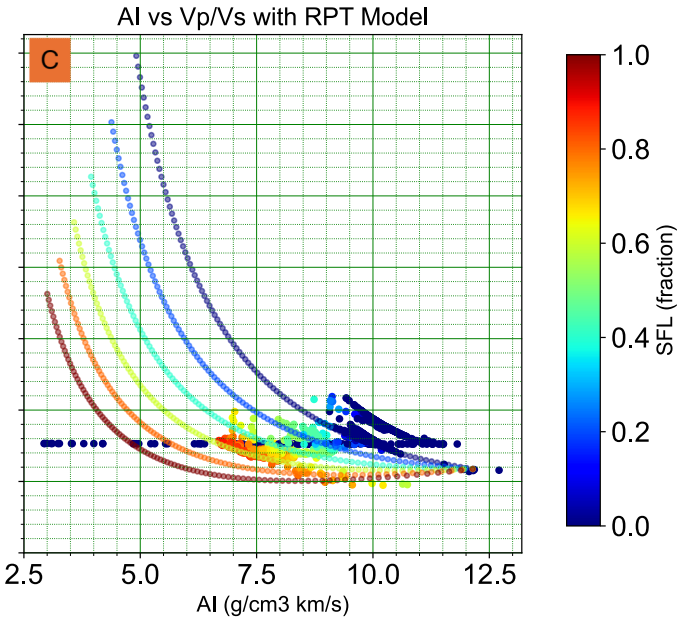

Figure 11. S_{FL} modelling using (A) density data, V_p data, and V_s data, (B) density data, V_p data, and scaled V_s model, and (C) density model, V_p model, and V_s model.

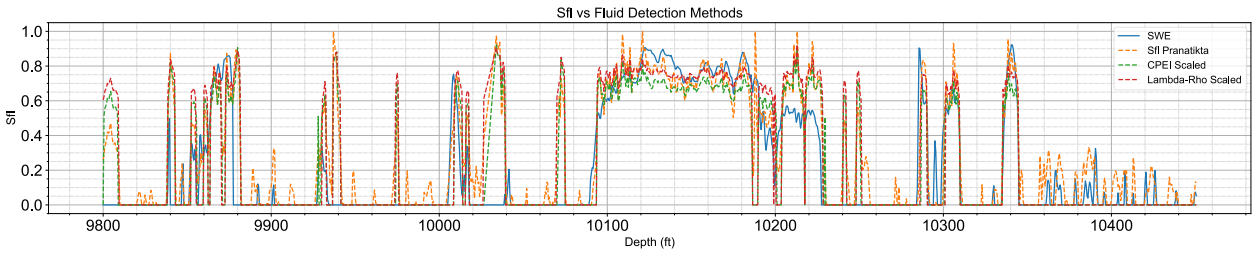

Figure 12. S_{FL} data (solid blue line) compared to Pranatikta and Winardhi (2025) RPT (orange dashed line), CPEI (green dashed line), and Lambda-Rho (red dashed line) in well SL-1.

CPEI, and Lambda–Rho, with values of 0.0970, 0.0983, and 0.1041, respectively. The detailed comparison is presented in Figure 12.

CONCLUSION

This study demonstrates that fundamental matrix parameters, specifically density and Vp, can be accurately derived using the MLR approach and effectively integrated into the Pranatikta and Winardhi (2025) RPT framework for fluid saturation modeling. The findings confirm that the Pranatikta and Winardhi (2025) RPT exhibits superior sensitivity to fluid saturation variations compared with conventional fluid-detection methods such as CPEI and Lambda–Rho.

These findings highlight the robustness of the proposed workflow and its potential to significantly improve fluid characterization, providing a viable solution for reservoirs with limited data availability. Furthermore, the proposed workflow provides a practical framework for applying the Pranatikta and Winardhi (2025) RPT in reservoirs where elastic and volumetric data are incomplete.

ACKNOWLEDGEMENT

The author would like to express sincere gratitude to the Bandung Institute of Technology (ITB) for providing the academic environment and institutional support that contributed to the successful completion of this research.

The author also acknowledges the support and guidance provided by colleagues and supervisors during the course of this study, as well as access to the data used in the analysis.

GLOSSARY OF TERMS AND SYMBOLS

Terms & Symbols	Definition	Unit
RPT	Rock physics template	
MLR	Multi-linear regression	
S_{FL}	Hydrocarbon fluid saturation fraction	0.Sfl
SW	Water saturation fraction	0.Sw
ϕ	Porosity	.fraction
ρ_b	Bulk density	gr/cc
ρ_{ma}	Matrix density	gr/cc
ρ_i	Density of rock-i	gr/cc
ρ_w	Density of water	gr/cc
ρ_{hc}	Density of hydrocarbon	gr/cc
V_i	Volumetric of rock-i	m/s
V_P	P-wave velocity	m/s
$V_{P_{fl}}$	P-wave velocity of fluids	m/s
V_{P_w}	P-wave velocity of water	m/s
$V_{P_{ma}}$	P-wave velocity in matrix condition	m/s
$V_{P\,hc}$	P-wave velocity of hydrocarbon	m/s
V_{P_i}	P-wave velocity of rock-i	m/s
V_S	S-wave velocity	m/s
$V_{S_{ma}}$	S-wave velocity in matrix condition	m/s
G	Fitting parameter of Pranatikta and Winardhi (2025) RPT	
n	Fitting parameter of Pranatikta and Winardhi (2025) RPT	
α	Ratio of S-wave matrix velocity and P-wave matrix velocity	
PEIL	Psuedo elastic impedance for lithology	
CPEI	Curved psuedo elastic impedance	
M	Empirical weighting component for AI	
N	Empirical weighting component fo Vp/Vs ratio in	
χ	Rotation angle	°

REFERENCES

Avseth, P., T. Mukerji, G. Mavko, & J. Dvorkin, (2010), Rock-Physics Diagnostics of Depositional Texture, Diagenetic Alterations, and Reservoir Heterogeneity in High-Porosity Siliciclastic Sediments and Rocks: A Review of Selected Models and Suggested Workflows. Geophysics 75 (5). https://doi.org/10.1190/1.348377.

Boruah, Nabajyoti, (2010), Rock Physics Template (RPT) Analysis of Well Logs for Lithology and Fluid Classification." In Proceedings of the 8th Biennial International Conference & Exposition on Petroleum Geophysics, Hyderabad, India.

Fawad, M., and N. H. Mondol, (2022), Monitoring Geological Storage of CO_2 Using a New Rock Physics Model. Scientific Reports 12 (1). https://doi.org/10.1038/s41598-021-04400-.

Gassmann, F., (1951), Elastic Waves through a Packing of Spheres. Geophysics 16: 673–685. https://doi.org/10.1190/1.143771.

Hutabarat, P, Bambang Widarsono, Fakhriadi Saptono, Humbang Purba, & Ridwan, (2014), Integrasi Inversi AVO dengan Model Analitik Petrofi sika untuk Menghitung Porositas dan Saturasi Air". Lembaran Publikasi Minyak dan Gas Bumi. DOI: https://doi.org/10.29017/ LPMGB.48.2.121.

Hutami, H., Tiara Larasati Priniarti, Ign. Sonny Winardhi, & Handoyo, (2019), Rock Physics Template To Esttimate The Effects of Total Organic Carbon (Toc) And Mineralogy on The Seismic Elastic Properties of Immature Shale Reservoir, Scientific contributions Oil and Gas, 42 (2) pp, 43-49 DOI: 10.29017/ SCOG. 42.2.43-49.

Lee, M.W., (2003), Velocity ratio and its application to predicting velocities. https:// doi.org/10.3133/ b2197.

Odegaard, E., and P. Avseth, (2004), Well Log and Seismic Data Analysis Using Rock Physics Templates. First Break 22 (10). https://doi.org/10.3997/1365-2397.200401.

Palgunadi, K. H., I. Viantini, S. Yogi, and S. Winardhie, (2016), A Novel Approach Comparison of Curved Pseudoelastic Impedance in Rock Physics Analysis. In SEG Technical Program Expanded Abstracts 2016, 3448–3452. Society of Exploration Geophysicists. https://doi.org/10.1190/segam2016-13850446.1.

Pangastuti, N. P. J. A. R., Mohammad Syamsu Rosid, and Edy Wijanarko, (2025), Binio Formation Characterisation Using Seismic Acoustic Impedance Inversion in the Lotus Field of the Central Sumatra Basin, Scientific Contributions Oil and Gas, 48 (2) pp. 95-110. DOI org/10.29017/scog.v48i2.1692.

Phani, K. K., and S. K. Niyogi. 1986. "Porosity Dependence of Ultrasonic Velocity and Elastic Modulus in Sintered Uranium Dioxide—A Discussion." Journal of Materials Science Letters 5: 427–430. https://doi.org/10.1007/BF0167235.

Pranatikta, K. A. & Winardhi I.S, (2025), Estimating Petrophysical Parameters from Acoustic Impedance and P to S Wave Velocity Ratio Using a Simple Rock Physics Model, First Break 43 (3): 61–70. https://doi.org/10.3997/1365-2397.fb202502.

Pranatikta, K. A., S. Winardhi, & R. A. Prastama, (2024), Direct Estimation of Petrophysical Properties from Elastic Parameters: A Case Study on the Batu Raja Formation. IOP Conference Series: Earth and Environmental Science 1437 (1): 012012. https://doi.org/10.1088/1755-1315/1437/1/01201.

Russell, B., (2015), Visualizing Inversion Results with Rock Physics Templates." In Inversion and Rock Physics Templates, CREWES Research Report 27. Consortium for Research in Elastic Wave Exploration Seismology (CREWES).

Ryannugroho, R., Sonny Winardhi, Djoko Santoso, Mohammad Rachmat Sule, Krishna Agra Pranatikta, Fernando Lawrens Hutapea, and Dona Sita Ambarsari, (2025), The Use of Modified Rock Physics Template to Monitor Fluid Saturation in Carbonate Reservoirs." Scientific Contributions Oil and Gas 48 (2): 217–237. https://doi.org/10.29017/scog.v48i2.1749.

Sukmono, S., and Ambarsari, D.S., (2019), Practical Seismic Interpretation for Petroleum Exploration. Bandung: ITB Press.

Taqiy, Z.F., Warto Utomo, Muhammad Shidqii, & Adi Susilo, (2025), Karakterisasi Reservoar Berdasarkan Analisis Inversi Seismik Impedansi Akustik dan Multiatribut Seismik, Studi Kasus: Lapangan Bunyu Tapa, Cekungan Tarakan, Kalimantan Utara. Lembaran Publikasi Minyak dan Gas Bumi.DOI: https://doi.org/10.29017/LPMGB.59.3.189.

Winardhi, Sonny, E. Dinanto, A. S. Sigalingging, R. Adityo, A. P. Utami, A. B. Ritonga, W. Satriawan, & Budiyono, (2023), Curved Pseudo Elastic Impedance Based on Elastic Attribute Rotation Scheme for Reservoir Petrophysical Property Prediction. IOP Conference Series: Earth and Environmental Science 1288 (1): 012026. https://doi.org/10.1088/1755-1315/1288/1/01202.

Wyllie, M. R. J., A. R. Gregory, & L. W. Gardner. 1956. "Elastic Wave Velocities in Heterogeneous and Porous Media." Geophysics 21: 41–70. https://doi.org/10.1190/1.143821.

Xu, S., & M. A. Payne, (2009), Modeling Elastic Properties in Carbonate Rocks. The Leading Edge 28 (1): 66–74.